2018 Spring Technical Meeting Central States Section of the Combustion Institute May 20–22, 2018 Minneapolis, Minnesota

Effect of Flow Duct Height on Concurrent-Flow Flame Spread and the Near-Limit Oscillation

Yanjun Li^{1,*}, Ya-Ting T. Liao¹, and Paul V. Ferkul²

¹Department of Mechanical and Aerospace Engineering, Case Western Reserve University, Cleveland Ohio, 44106, USA ²Universities Space Research Association, Cleveland Ohio, 44135, USA *Corresponding Author Email: yxl1453@case.edu

Abstract: Concurrent flame spread over a thin solid material in a low-speed flow duct in microgravity is numerically studied using a three-dimensional transient CFD code. The height of the flow duct is the main parameter in this study. The preliminary results show that there exists a quenching flow duct height below which the flame fails to spread. For cases far from the quenching height, the flame reaches a steady spreading state before the sample is consumed. The flame spread rate and the pyrolysis length at steady state first increases then decreases when the flow duct height increases. Near the quenching height, a flame oscillation is observed throughout the flame spreading process. As it spreads downstream, the flame goes through periodic lateral separation and merging while accelerating and decelerating. This flame oscillation phenomenon is suspected to be due to thermo-diffusive instability. Detailed profiles of the gas and solid phases, including the heat flux distributions on the sample surfaces, interactions between the flame and the walls of the flow ducts, and the flow profiles are examined to elucidate the underlying physics of the observed phenomena. Keywords: Tunnel height effect, microgravity combustion, concurrent flame spread, near quenching oscillation

1. Introduction

Fires in confined spaces (e.g., buildings, transportation vehicles, tunnels) are a major safety concern. They result in significant numbers of injuries, civilian deaths, and property losses every year [1]. In confined spaces, fire behaviors can be very different from fires in open spaces. To address this concern, many past studies have focused on the mechanical (or aerodynamic) interactions between structures and fires, using stationary burners in rooms, corners, tunnels, or near walls [2, 3, 4, 5]. Other studies have focused on tunnel fires with ventilated flows [6, 7, 8, 9, 10, 11, 12, 13]. In most of these studies, fires are simulated experimentally using stationary burners – the flame does not move. However, in most situations, real fires in confined spaces involve flames that themselves move or spread across the fuel.

Flame spread is one of the most important characteristics of a fire, as it determines the available time to control the fire or to escape the area. There have been tremendous efforts on studying flame spread over solid materials using microgravity experiments. In microgravity, buoyancy is essentially eliminated and hence forced flow can be imposed on the sample independent of other parameters. For concurrent-flow flame spread in microgravity, limiting flame lengths and steady spread rates were predicted by numerical models [14, 15]. They were also verified in space

experiments such as BASS where thick plastic rods [16] and thin fabric samples [17] were burned in low-speed concurrent flows in a small duct.

In a recent NASA-led project (Saffire), a series of large-scale flame spread experiments were conducted in unmanned International Space Station (ISS) re-supply vehicles prior to their destructive reentry in Earth's atmosphere [18]. These experiments were approximately ten times larger (lengths of the flow duct and samples are ~1m) than prior experiments. Results yielded significantly smaller flame spread rates than seen in previous smaller-scale experiments for the same thin fabric, even though all other environmental conditions were the same (oxygen, pressure, and flow speed). This observation that flames spread faster in smaller ducts (e.g. BASS) is suspected to be due to thermal expansion during combustion which causes acceleration because the flow is more confined. This is referred to as the channeling effect. The increased radiation heat feedback from duct walls to the flame and to the fuel surface may also be a factor.

Several research groups have numerical studies that address this situation. For instance, an earlier simulation using a steady two-dimensional model (capable of only finding steady-state solutions) by Shih and T'ien showed that the concurrent flame spread rate increases as the tunnel height decreases [19], consistent with the experimentally observed phenomena. However, in their simulation, Shih and T'ien showed that when the tunnel height is very small, conductive heat loss to the tunnel walls increases, slowing the spread rate. This eventually leads to flame quenching. Their results also show that for the same tunnel height, the flame becomes longer and the spread rate increases when the reflectivity of the tunnel wall increases. No steady state solution was achieved for wall reflectivity of \sim 1. It is suspected that the flame continuously accelerates while traveling downstream (a transient process).

We conduct numerical investigations to study fire behaviors and flame spread in confined spaces. These are performed in advance of an upcoming microgravity experiment that will examine concurrent-flow flame spread over flat samples in a small flow duct aboard the ISS. A wide range of parameters will be tested, including duct height, sample material, duct wall surface properties, flow speed, and oxygen concentration. For the numerical effort, a combustion CFD code is used to simulate this transient process. In this paper, we will introduce the concept of the experiments and present the preliminary results of our numerical simulation.

2. Microgravity Experiment

The new flame spread experiment aboard the International Space Station will leverage the existing BASS (Burning and Suppression of Solids) wind tunnel facility. NASA's previous BASS and BASS-II projects examined the burning and extinction characteristics of various solid fuel samples in microgravity. Flat, cylindrical, and spherical samples of different materials were burned in concurrent, opposed, or stagnation flow configurations in a small flow duct situated in the Microgravity Science Glovebox (MSG) aboard the ISS [20, 16, 17, 21]. The flow duct has a cross-sectional area of 7.6 cm × 7.6 cm and a length of 20 cm (see Fig. 1a).

In one series of BASS tests, concurrent flame spread over a thin composite fabric blend (SIBAL) were studied. Samples (1.2 or 2.2 cm wide, 10 cm long) were mounted in a stainless steel sample holder in the flow duct and were ignited by a hot wire at the leading edge (see Fig. 1b). These tests were conducted in various ambient oxygen percentages (molar fraction 16-21%) and with different forced flow velocities (1-55 cm/s). Ambient pressure was 1 atm. The flame growth process was recorded on video (at 29.97 frames/second) and using a digital still camera (one image every ~1.2s) from outside the flow duct through windows.

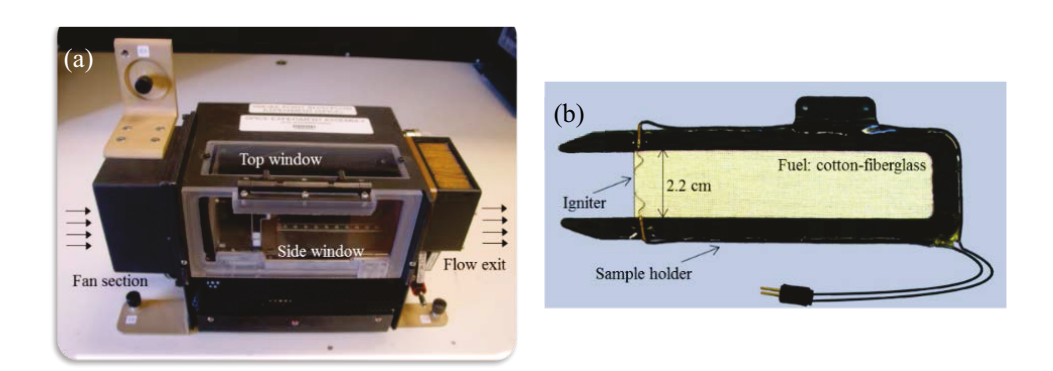


Figure 1: BASS wind tunnel facility [17]. (a) Small flow duct. (b) Fuel sample, sample holder, and igniter.

In this work, we plan to vary the tunnel height, fuel type, wall properties, flow speed, and oxygen concentration. The main source of data will be derived from digital images of the flame from which we can measure flame size, growth, spread rate, and quenching.

We propose to create an effective reduction in the height of the tunnel by adding two baffles parallel and adjacent to the fuel sample, one on each side of the sample (see Fig. 2). The baffles will be mounted on an adjustable rack so that the distance between the baffles (D_b) can be changed in 0.5-cm increments between 0 and 7.6cm. This will allow us to explore the limiting quenching distance and to precisely determine the regimes of steady and accelerating flames (if they exist). We also propose to use baffles with different surface treatments, simulating different radiative wall properties. Examples include transparent glass, blackened aluminum (reflectivity \sim 0), and polished metal (reflectivity \sim 1). This allows us to investigate the radiative interactions between the tunnel wall and the spreading flame.

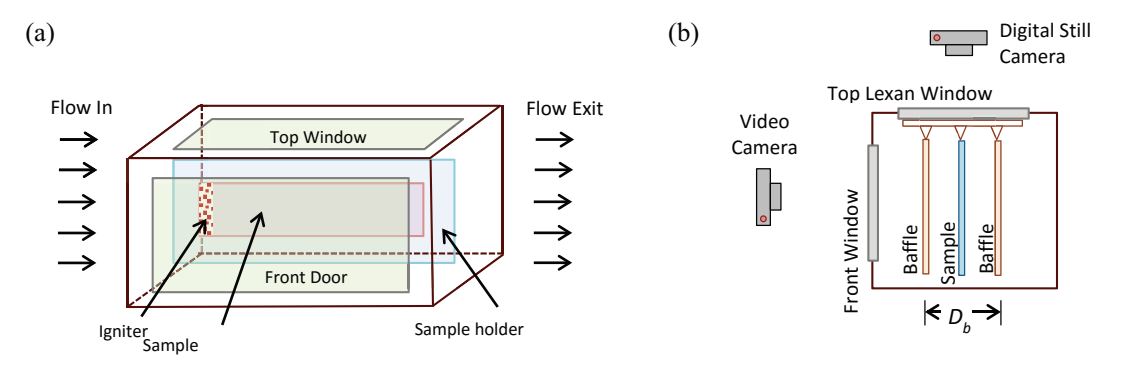


Figure 2: Experimental setup (not to scale). (a) Three-dimensional view. (b) Edge view from the tunnel exit. Note: baffles are not shown in (a).

For the sample selection, we will rely on the fuel sample concept used in the BASS project. Flat thin PMMA slabs (thickness: 1mm or less) and SIBAL fabric will be tested. The igniter will be integrated into each sample for a one-time use. The testing conditions will be 15 to 21% oxygen at 1 atm. The flow speeds of interest are 0 to 30 cm/s.

3. Numerical Model

The numerical model used in this work is based on a previously developed three-dimensional transient CFD model. The detailed information and formulation has been described in other studies [22, 23, 24].

The configuration of the model is based the flow duct and sample setup in BASS (see Fig. 3 and Table 1). The height of the flow duct (H) is a parameter in this study. It varies between 7.6cm (corresponding to BASS) and 1cm. The fuel sample, SIBAL (75% cotton and 25% fiberglass) is sandwiched by a sample holder and is placed at the center of the flow duct. Air flow at 10 cm/s is imposed at the duct inlet. Ignition is achieved by applying external heat flux at the upstream leading edge of the sample. After ignition, the external heat flux is gradually turned off in 3 seconds. To allow sufficient time for flame development, the sample length is set to 30cm (instead of 10cm in BASS) in the simulations. This facilitates observation of the eventual fate of the flame (accelerating flame spread, steady flame spread, or extinction). The ambient conditions are at zero gravity with temperature of 300K and pressure of 1atm.

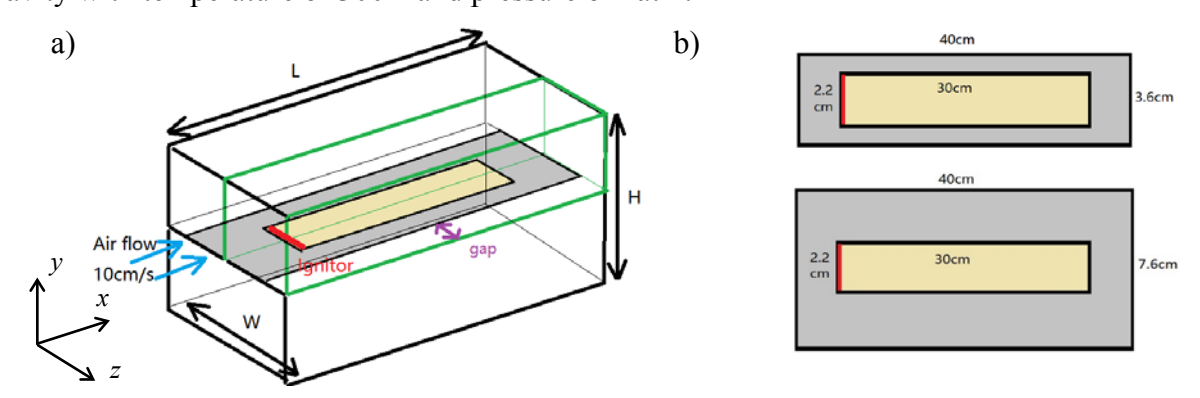


Figure 3: Model configuration (a) Sample, sample holder, and the flow duct. (b) Sample and sample holder (not to scale)

=	Tunnel size (W×L×H)	Sample holder size (W×L)	Sample size (W×L)	Sample distance to tunnel entrance	Sample distance to tunnel exit
	7.6×40×h*	3.6×40 (with gaps on the sides)	2.2×30	5	5

Table 1: Dimensions of sample and flow duct (unit: cm)

*h=1, 2, 4, 7.6 (cm).

In the simulations, two sample holders with different width (W) are considered. One sample holder has the same width as the flow duct. Another sample holder is narrower than the flow duct, leaving 2cm gaps between the edges of the sample holder and the duct side walls (see Fig. 3a). The sample setup has an effect on the flow profile when the flow duct height is on the order of the flow boundary layer thickness. Figure 4 shows the flow profiles on the mid cross-section of the flow duct. For the BASS flow duct (H=7.6cm), it is clear that the boundary layer grows on the walls of the flow duct as well as on the surface of the sample holder. The effective area for the flow passage is reduced, resulting in flow speeds higher than the inlet velocity (10cm/s) in the area between the sample holder and the ceiling of the flow duct. The maximum flow velocity increases when the height of the flow duct decreases. However, for the sample setup with the narrow sample holder, the 2cm side gaps ventilate most of the flow. In the area between the sample holder and

the flow duct ceiling, the flow is 'locked' by the viscous boundary layer. In other words, the flow that the fuel sample encounters is significantly lower than the airflow imposed at the duct inlet. This has a significant impact on the flame spread process and will be discussed further below.

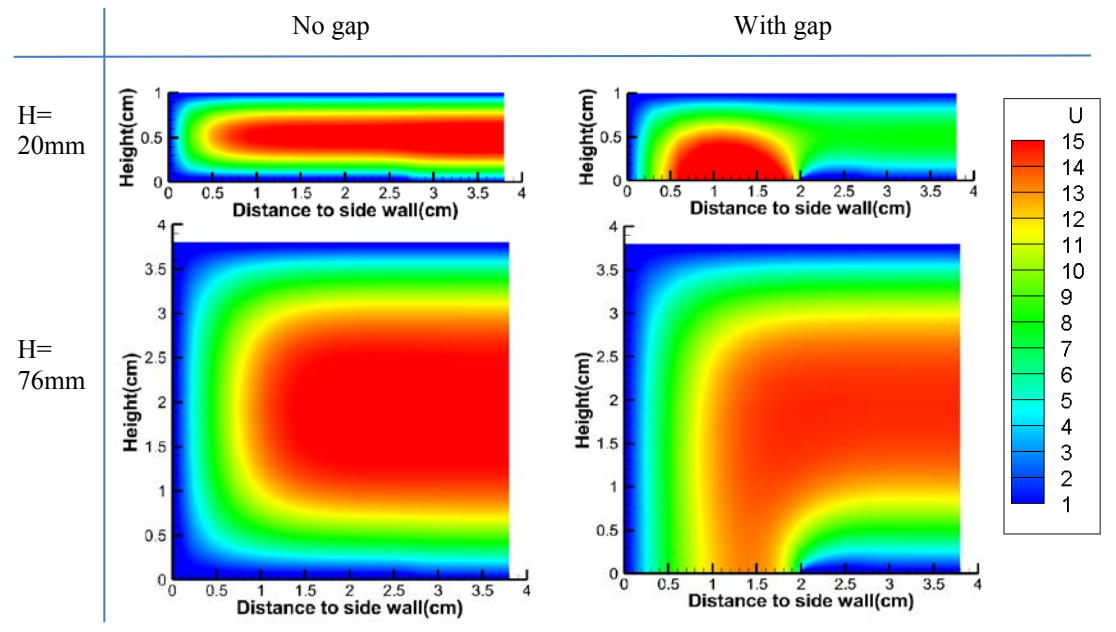


Figure 4: Flow velocity profile on the mid cross-section of the flow duct (x=20cm). Flow velocity at the flow duct inlet: 10cm/s. Results are from pure flow without combustion. The y-axis "Height" is the distance from the sample surface.

In the simulation, symmetry is assumed on the plane along the centerline of the fuel sample and on the plane of the sample half-thickness. This reduces the computational domain to a quarter of the flow duct (marked by the green lines in Fig. 3). The model employs a non-uniform grid structure and an automatic Adaptive Mesh Refinement (AMR) scheme. The program traces the flame location and allocates fine meshes (one-tenth of the characteristic length for thermal diffusion) in the regions near the flame base and pyrolysis tip while the flame spreads downstream.

4. Preliminary Numerical Results

In most of the simulated cases, steady spread was observed. Figure 5 shows the advancement of the sample burning region for H=2cm. The burning region is defined as solid pyrolysis reaction rate >10⁻⁵ g/cm²/s. Results of both sample setups (with and without the side gaps) show that after an initial transient period, the flame reaches a limiting length and spreads downstream with a constant spread rate. For the sample setup with the side gaps, the flame is shorter and spreads slower compared to the setup without the side gaps. This is because the flame encounters a smaller flow as explained above.

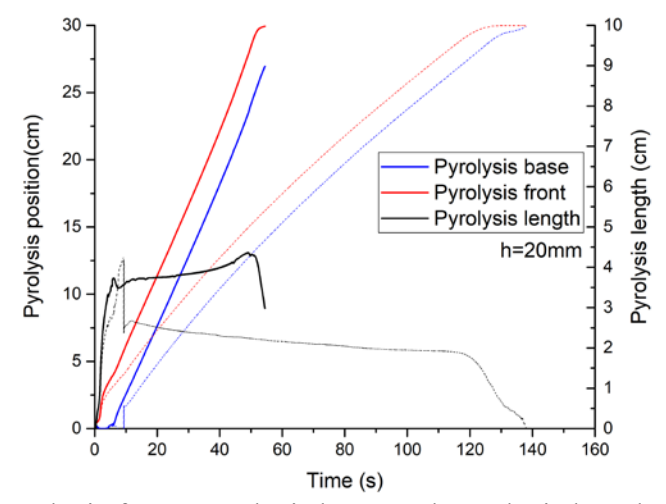


Figure 5: Location of pyrolysis front, pyrolysis base, and pyrolysis length versus time for h=20mm. Dashed lines denote results for sample setup with side gaps. Solid thick lines denote results for sample setup without side gaps.

4.1 Effect of the height of the flow duct

The steady-state pyrolysis lengths and spread rates are plotted against flow duct height in Fig. 6. For both sample setups, the pyrolysis length and spread rate first increase and then decrease when the flow duct height is reduced. Among the simulated cases, the optimal flow duct height for the flame spread occurs at 30 to 40mm. When the flow duct height is below a critical value, the flame fails to spread to the end of the sample.

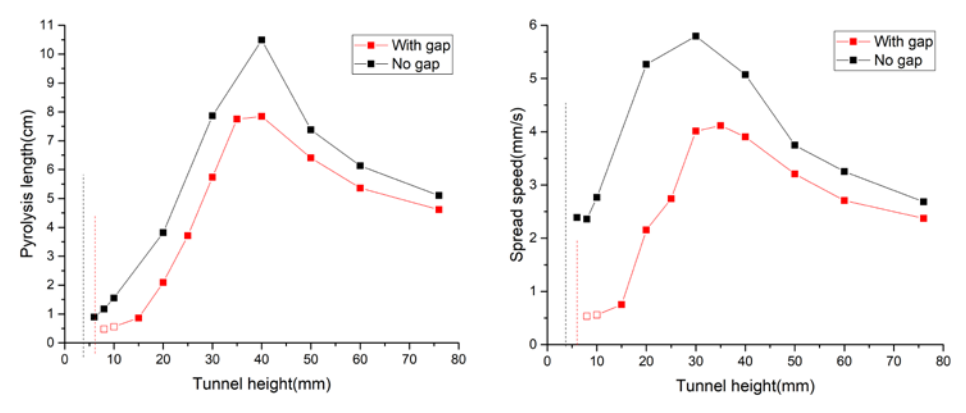


Figure 6: Pyrolysis length and spread rate for flow duct with different heights. The dash lines denote the quench limits. Hollow symbols denote partial propagation.

To understand this non-monotonic trend, solid and gas profiles are examined in detail. Figures 7 and 8 compare the oxygen profiles on the center symmetry plane and the heat flux distributions on the sample surface and duct ceiling. For these profiles, the two sample setups have similar results and hence only results for the sample setup with side gaps are shown here.

When the duct height is sufficiently large (e.g., h=4cm), oxygen is transported (via convection and diffusion) to the downstream end of the duct. When the duct height is small (e.g., h=2cm), the flame extends to the ceiling, shielding the downstream region from the oxygen. The reduced

oxygen supply to the flame and to the downstream region may contribute to the shorter pyrolysis length and the smaller spread rate for h=2cm compared to h=4cm.

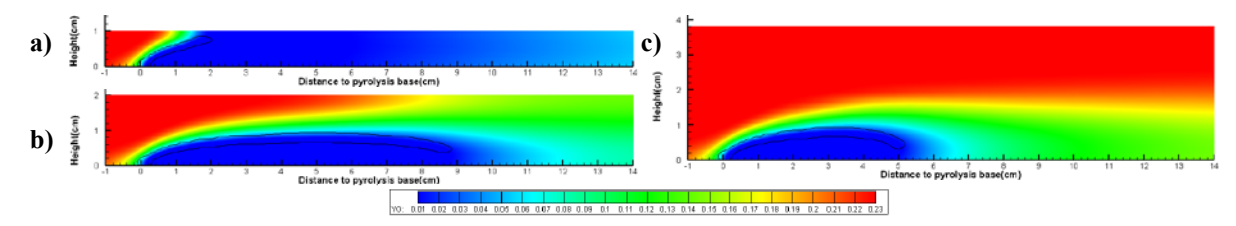


Figure 7: Mass fraction of oxygen on the center symmetry plane. a) h=2cm. b) h=4cm. c) h=7.6cm. Black contour: gas phase reaction at 10^{-4} g/cm³/s.

Figure 8a shows the conductive and radiative heat fluxes on the sample surface and the duct ceiling for h=2cm. Figure 8b-c further compares the heat fluxes along the centerline of the sample for different duct heights. The heat fluxes for h=4cm and h=7.6cm are of similar magnitudes. Conductive heat to the ceiling is negligible as the flame is far away from the ceiling. The heat loss to the ceiling is mainly due to flame radiation. At h=2cm, the flame is in close proximity to the duct ceiling (see Fig. 7a). Thus, the conductive heat loss to the ceiling becomes much larger and is comparable to the conductive heat feedback to the sample surface. Also note that the peak of the conductive heat loss to the ceiling is near the flame front. At h=2cm, the radiation heat loss to the ceiling is also approximately two times higher than with h=4cm and 7.6cm.

To summarize, when the duct height decreases, the oxygen supply to the flame reduces and the heat losses to the duct ceiling increase. These two effects result in a weak flame and eventually lead to flame quenching when the duct height is sufficiently small (below a quenching height).

The velocity profiles and flame shape at the center symmetry plane are examined in Fig. 9. It is evident that in all cases, the flow accelerates due to the thermal expansion during the combustion process. This effect is more significant when the duct height is small. Compared to h=7.6cm (Fig. 9c), the flow for h=4cm (Fig. 9b) is stronger, and as a consequence, the flame is longer. However, when the duct height is further reduced, the flow is diverted to the side gaps (if present). The flow speed on the center symmetry plane is low even after thermal expansion (e.g. h=2cm; left of Fig. 9a). This effect, in addition to the reduced oxygen supply and the increased heat loss to the ceiling, contributes to the decreased spread rate and pyrolysis length when duct height decreases. Note that both the quenching height and the optimal duct height for flame spread are slightly higher for sample setups with side gaps compared to those without gaps.

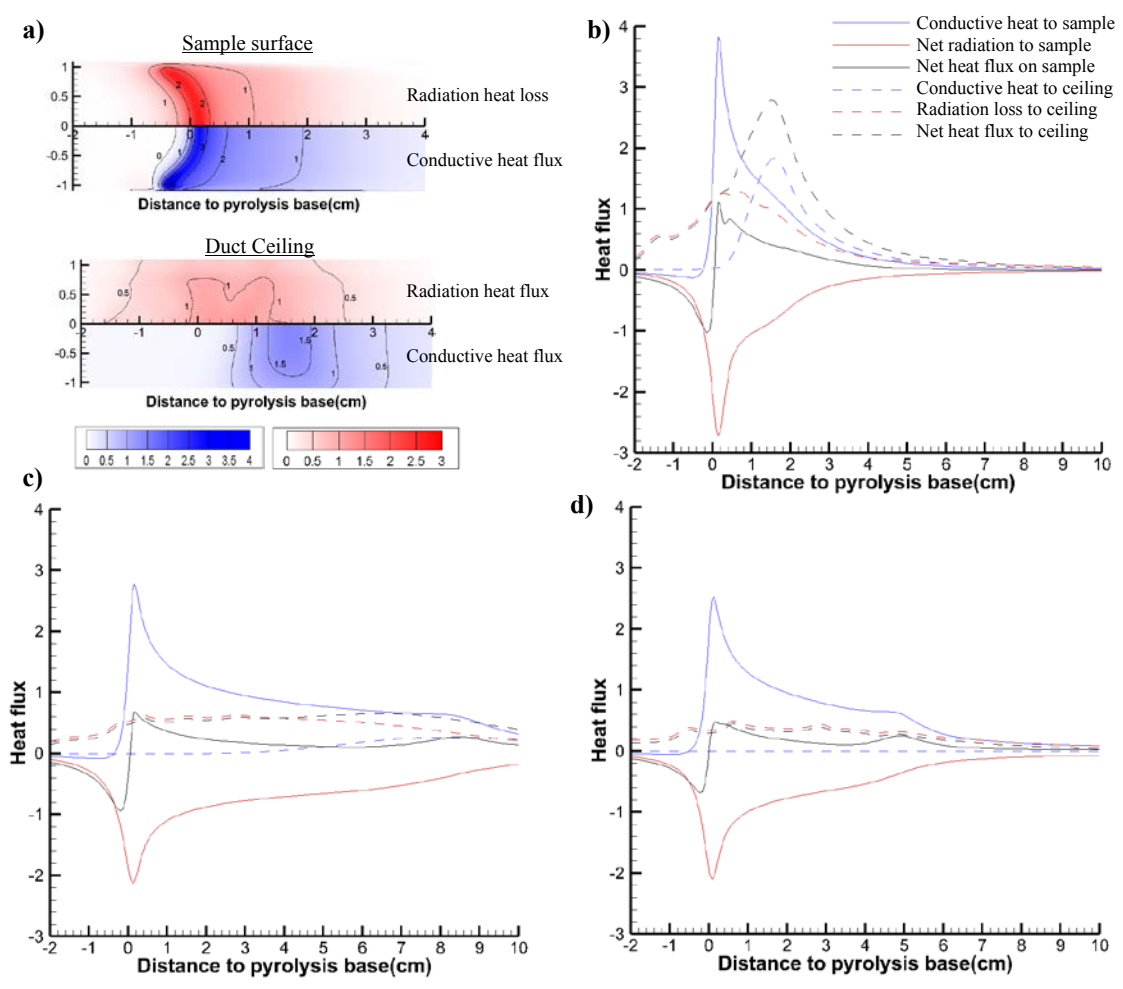


Figure 8: Conductive and Radiative heat fluxes a) distributions on the sample surface and duct ceiling for h=2cm. b) –d) Along the sample centerline for h=2cm, 4cm, and 7.6cm respectively.

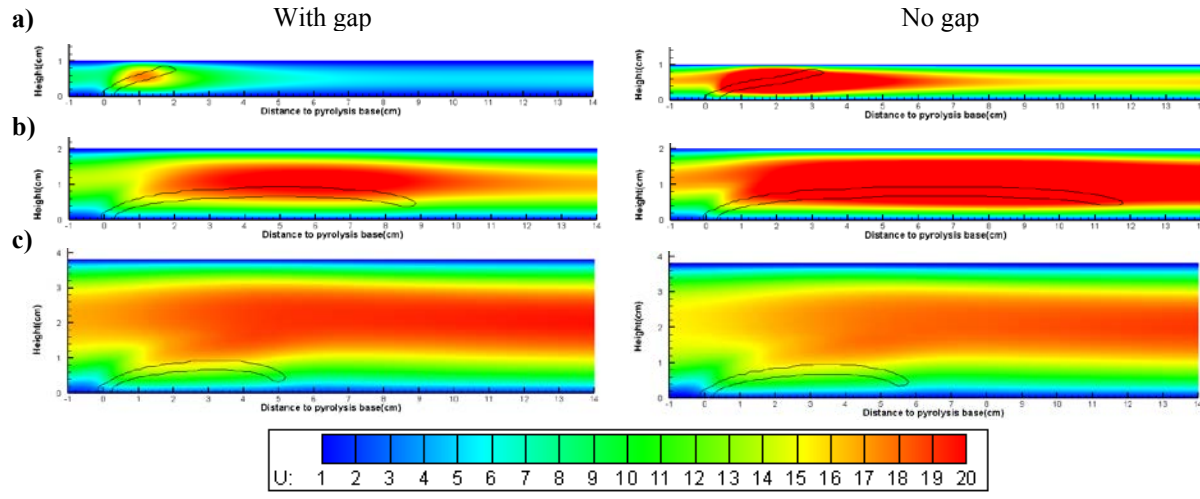


Figure 9: Flame shape (fuel vapor reaction rate $=10^{-4}$ g/cm³/s, shown as black contour) and flow velocity in the stream direction. a) h=2cm. b) h=4cm. c) h=7.6cm

4.2 Near limit oscillation

As mentioned above, there exists a quenching duct height below which no flame spread is observed. Near this limit, the pyrolysis length was observed to oscillate for sample setups with gaps (Fig. 10a). The maximum gas temperature and its location relative to the pyrolysis base also exhibit in-phase oscillations (Fig. 10b). This phenomenon was reported in previous works for candle flames [25], edge flames [26], pool fire [27], opposed-flow diffusion flames [28, 29] and concurrent-flow diffusion flame [30]. It was attributed to thermo-diffusive instability.

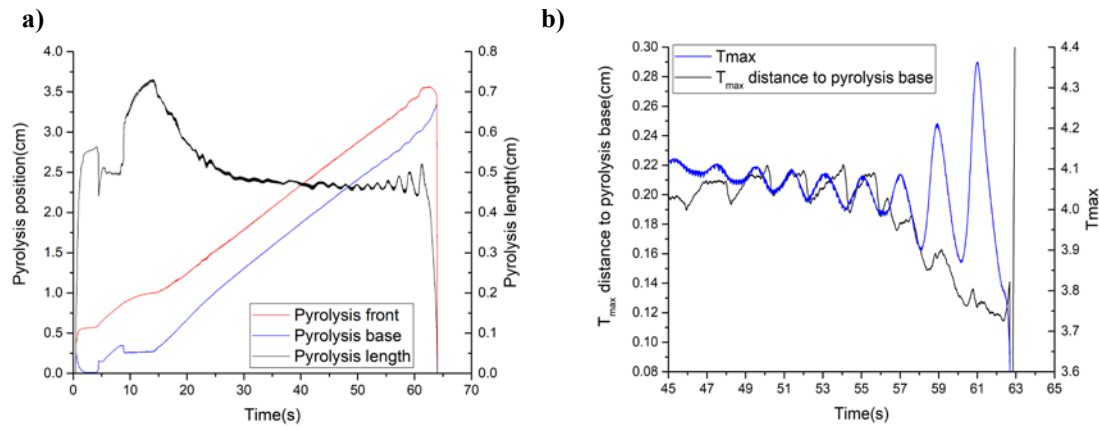


Figure 10: Near quenching oscillation. a) Location of pyrolysis front, pyrolysis base, and pyrolysis length on the center symmetry plane. b) Maximum gas temperature and its position relative to the pyrolysis base. (h=8mm with sample setup with side gaps).

The period of the oscillation in Fig. 10 is \sim 2s. The flame and solid profiles in one period are examined. The flame splits and merges in the lateral (cross stream) direction. In the first half of one period, two flamelets near the sample sides grow laterally and merge at the center. In the second half of the period, the flame splits laterally and forms two flamelets. Then, the next period starts. This interesting phenomenon warrants further investigations in our future work.

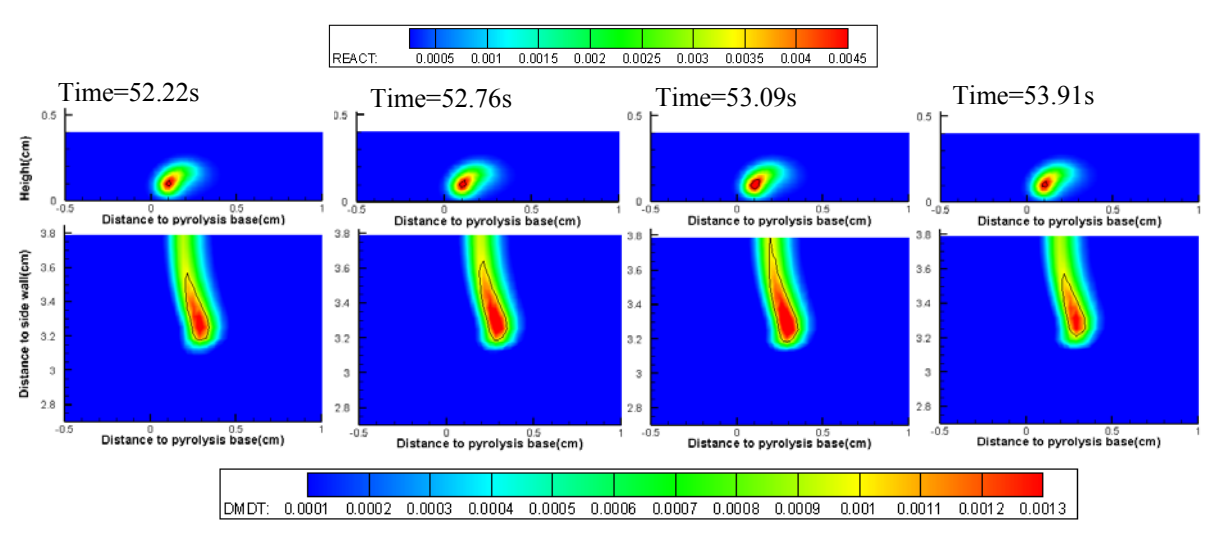


Figure 11: One cycle or period of fire oscillation. Top: Reaction rate at the center symmetry. Units: g/cm³/s. The solid line denotes reaction rate 0.0045g/cm³/s. Bottom: Mass loss rate on solid surface. Units: g/cm²/s. The solid line denotes reaction rate 0.001g/cm²/s

9

5. Conclusions

This work utilizes a comprehensive numerical model to study the effect of confinement on flame spread and the flame-wall aerodynamics/thermal interactions. These are done in support of upcoming microgravity experiments aboard the ISS. Tests of concurrent-flow flame spread over flat samples will be conducted in an existing flow duct (BASS facility). A wide range of parameters will be tested, including duct height, sample material, duct wall surface properties, flow speed, and oxygen concentration.

A three-dimensional transient CFD code was also used to simulate this process. The height of the flow duct is the main parameter in this study. The main findings from the preliminary simulation results are:

- 1) In most simulated cases, the flame reaches a steady spreading state before the sample is consumed. The flame spread rate and the pyrolysis length at steady state first increases then decreases when the flow duct height decreases.
- 2) The flow confinement imposed by the duct has multiple effects on the flame spreading process. On one hand, it accelerates the flow when the flow experiences thermal expansion during combustion. This intensifies the flame. On the other hand, it limits the oxygen supply to the flame. Flame also loses heat to the duct walls through conduction. These reduce the strength of the flame. These competing effects results in the above-mentioned non-monotonous trend of the flame spread rate at different duct heights.
- 3) When the duct height is in the order of the thickness of the flow viscous boundary layer, the setup of the sample plays a significant role on the experiment. In our cases, a flat thin sample is placed in the center of the flow duct and it (or its holder) does not span across the width of the duct, leaving gaps on the two sides. Flow is diverted to the side gaps and the actual flow speed in the sample region is significantly lower than the flow imposed at the duct inlet. This will reduce the flammability of the sample.
- 4) When the height of the duct is below a quenching limit, no flame spread is observed. Near this limit, oscillation of the pyrolysis length was observed. The flame splits and merges periodically in the lateral direction before the flame dies. This phenomenon is suspected to be due to the thermo-diffusive instability and will be investigated further in our future work.

6. Acknowledgements

This work is supported by National Science Foundation under grant number CBET-1740478. The authors would also like to thank CASIS (Center for the Advancement of Science in Space) and ZIN Technologies for the technical support on the microgravity experiments. This work made use of the High Performance Computing Resource in the Core Facility for Advanced Research Computing at Case Western Reserve University.

7. References

- [1] H.J.G. Haynes, "Fire Loss in the United States During 2015," National Fire Protection Association, 2016.
- [2] B.Y. Lattimer and U. Sorathia, Fire Safety Journal 38 (2003) 709-745.
- [3] B.Y. Lattimer and U. Sorathia, Fire Safety Journal 38 (2003) 747-770.
- [4] M. Poreh and G. Garrad, Fire Safety Journal 34 (2000) 81-98.

- [5] O. Megret and O. Vauquelin, Fire Safety Journal 34 (2000) 393-401.
- [6] L.H. Hu, R. Huo, H.B. Wang, Y.Z. Li and R.X. Yang, Building and Environment 42 (2007) 3905-3915.
- [7] L.H. Hu, W. Peng and R. Huo, Journal of Hazardous Materials 150 (2008) 68-75.
- [8] J.S. Roh, S.S. Yang, H.S. Ryou, M.O. Yoon and Y.T. Jeong, Building and Environment, 43 (2008) 1225-1231.
- [9] H. Ingason and Y.Z. Li, Fire Safety Journal, 45 (2010) 371-384.
- [10] J.P. Kunsch, Fire Safety Journal, 37 (2002) 67-81.
- [11] M. Weng, X. Lu, F. Liu and C. Du, Applied Thermal Engineering, 94 (2016) 422-434.
- [12] F. Tang, L. Li, M. Dong, Q. Wang, F. Mei and L. Hu., Applied Thermal Engineering, 110 (2017) 1021–1028.
- [13] X. Tian, M. Zhong, C. Shi, P. Zhang and C. Liu, Applied Thermal Engineering, 116 (2017) 233–243.
- [14] P.V. Ferkul and J.S. T'ien, Combust. Sci. and Technology, 99 (1994) 345-370.
- [15] Y.-T. Tseng and J.S. T'ien, Journal of Heat Transfer, 132 (2010) 091201.
- [16] S.L. Olson and P.V. Ferkul, "Microgravity Flammability of PMMA Rods in Concurrent Flow," in 9th US National Combustion Meeting, Cincinnati Ohio, 2015.
- [17] X. Zhao, Y.-T. T. Liao, M.C. Johnston, J.S. T'ien, P.V. Ferkul and S.L. Olson, Proc. Combust. Inst., 36 (2017) 2971-2978.
- [18] G. Jomas, J.L. Torero, C. Eigenbrod, J. Niehaus, S.L. Olson, P.V. Ferkul, G. Legros, A.C. Fernandez-Pello, A.J. Cowlard, S. Rouvreau, N. Smirnov, O. Fujita, J.S. T'ien, G.A. Ruff and D.L. Urban, Acta Astronautica, 109 (2015) 208-216.
- [19] H.-Y. Shih and J.S. T'ien, "Modeling Wall Influence on Solid-Fuel Flame Spread in a Flow Tunnel," in 35th Aerospace Science Meeting & Exhibit, Reno, NV, 1997.
- [20] S.L. Olson, P.V. Ferkul, S. Bhattacharjee, F.J. Miller, C. Fernandez-Pello, S. Link, J.S. T'ien and I. Wichman, "Results from on-board CSA-CP and CDM Sensor Readings during the Burning and Suppression of Solids II (BASS-II) Experiment in the Microgravity Science Glovebox (MSG)," in 45th International Conference on Environmental Systems, Bellevue, Washington, 2015.
- [21] S. Bhattacharjee, A. Simsek, O. Sandra and P. Ferkul, Combust. Flame, 163 (2016) 472-477.
- [22] X. Zhao, Y.-T. T. Liao, M.C. Johnston, J.S. T'ien, P.V. Ferkul and S.L. Olson, Proc. Combust. Inst., 36, (2017) 2971-2978.
- [23] X. Zhao and J.S. T'ien, Combust. Flame, 162 (2015) 1829-1839.
- [24] Y.-T.T. Liao and J.S. T'ien, Combust. Theory and Modelling, 17 (2013) 1096-1124.
- [25] D. Dietrich, H. Ross, Y. Shu, P. Chang and J. T'ien, Combust. Sci. and technology, 156 (2000) 1-24.
- [26] J. Buckmaster and Y. Zhang, Combustion Theory and Modelling, 3 (1999) 547-565, 1999.
- [27] D.N. Schiller, H.D. Ross and W.A. Sirignano, Combust. Sci. and Technology, 118 (1996) 203-255.
- [28] K. M. N. Kumar and A. Kumar, Proc. Combust. Inst., 36 (2017) 3081-3087.

- [29] S.L. Olson, F.J. Miller, S. Jahangirian and I.S. Wichman, Combust. Flame, 156 (2009) 1214-1226.
- [30] S. Wang, S. Wang, K. Zhu, Y. Xiao and Z. Lu, Combust. Sci. and Technology, 188 (2016) 451-471.